

Quantifying the Importance of Soil Forming Factors Using Multivariate Soil Data at Landscape Scale

Andre Eger¹, Nina Koele¹, Thomas Caspari¹, Matteo Poggio², Kumar Kishor¹, and Olivia Rata Burge¹

¹Manaaki Whenua - Landcare Research

²Helmholtz Centre for Environmental Research (UFZ)

November 21, 2022

Abstract

The role of soil forming factors (time, parent material, climate, biota, topography) on soil processes has commonly been studied using soil sequences where only one factor varies between sites. However, when multiple factors change, it becomes difficult to partition the importance of different soil forming factors for soil formation. We show for an altitudinal gradient how proximal sensing (portable XRF, Fourier-Transform Infrared [FTIR]), multivariate statistics and Bayesian mixing modelling can help to quantify the importance of two soil forming factors. First, we confirmed the existing qualitative soil-landscape model of concomitant shifts in parent material (greywacke loess to mafic volcanics) and climate (higher precipitation) with altitude, leading to increases in pedogenic oxides, soil carbon, and soil Fe, while Si concentrations and pH declined. Second, we applied a mixing model using immobile elements as parent material tracers to quantify the parent material contribution in soils across our gradient. Third, we conducted a variation analysis to determine how much variation in the soil FTIR spectra could be explained by parent material and climate. Parent material alone explained 31% of the variation, climate alone only 9%. However, if we had only considered climate as explanatory variable, it would have accounted for almost half of the total variation (41%) because of the strong interaction between climate and parent material, and therefore concealing the leading role of parent material. Given that parent material is often omitted in modern digital soil mapping, our results emphasize the importance of parent material as a predictor of spatial soil distribution.



Journal of Geophysical Research – Earth Surface

Supporting Information for

Quantifying the Importance of Soil Forming Factors Using Multivariate Soil Data at Landscape Scale

Eger¹, N. Koele², T. Caspari¹, M. Poggio³⁺, K. Kumar³, and O. R. Burge⁴

¹Manaaki Whenua – Landcare Research, Soils & Landscapes, Lincoln 7608, New Zealand

²Manaaki Whenua – Landcare Research, Land Use & Ecosystems, Lincoln 7608, New Zealand

³Manaaki Whenua – Landcare Research, Land Use & Ecosystems, Palmerston North 4474, New Zealand

⁴Manaaki Whenua – Landcare Research, Ecosystems & Conservation, Lincoln 7608, New Zealand

Corresponding author: A. Eger, egera@landcareresearch.co.nz

+current address: Helmholtz-Zentrum für Umweltforschung, Department of Soil System Science, 06120 Halle, Germany

Introduction

The supplement contains:

a list of all script and data files used in the study; these files are supplied separately through <https://datastore.landcareresearch.co.nz/dataset/jgr-soilformingfactors>;

all supplementary figures referenced in the main text.

Additional files supplied separately

BanksP_chemistry.R

R code for Figure 2 using the data in ‘BanksP_lab_paper.xlsx’

BanksP_mixing.R

R code for performing Bayesian mixing model using the following input files: ‘mixdata_reduced.csv’, ‘pm_reduced_means.csv’, ‘discr.csv’; analysis produces output files ‘diagnostics.txt’, ‘summary_statistics.txt’, ‘BP_model_1.txt’ that were summarized to create ‘mixing_results.xlsx’;

Data from ‘mixing_results.xlsx’ and ‘BanksP_lab_paper.xlsx’ was used to create Figure 4 and 5

BanksP_FTIR.R

R code for statistical analysis of FTIR based on FTIR data in ‘MIR_Banks_spectra_abs_ID.csv’; used to create Figure 3

BanksP_pm.R

R code for visualizing parent material and immobile element data in Figure S1 and S3, using data from ‘BanksP_lab_paper.xlsx’ and ‘pm_paper.xlsx’

BanksP_var.R

R code for variation partitioning using ‘MIR_Banks_spectra_abs_ID.csv’, ‘mixing_results.xlsx’ and ‘BanksP_lab_paper.xlsx’ as input data; output of analysis is used for Figure S2

- List of data files (soil data, parent material data, input and output files related to statistical and mixing modelling):
- ‘BanksP_lab_paper.xlsx’ – site and soil analytical data, including pXRF data
- ‘MIR_Banks_spectra_abs_ID.csv’ – FTIR absorbance data for soil sites; note that sample LAB_ID = “M185028” was accidentally not scanned
- ‘pm_paper.xlsx’ – parent material data from external references
- ‘mixdata_reduced.csv’ – input data for Bayesian mixing model derived from ‘BanksP_lab_paper.xlsx’
- ‘pm_reduced_means.csv’ – input data for Bayesian mixing model derived from ‘pm_paper.xlsx’
- ‘discr.csv’ – input file for Bayesian mixing model
- ‘diagnostics.txt’, ‘summary_statistics.txt’, ‘BP_model_1.txt’ – output files of Bayesian mixing model
- ‘mixing_results.xlsx’ – summary of Bayesian mixing model results used for further analysis

Supplementary figures referenced in the main text

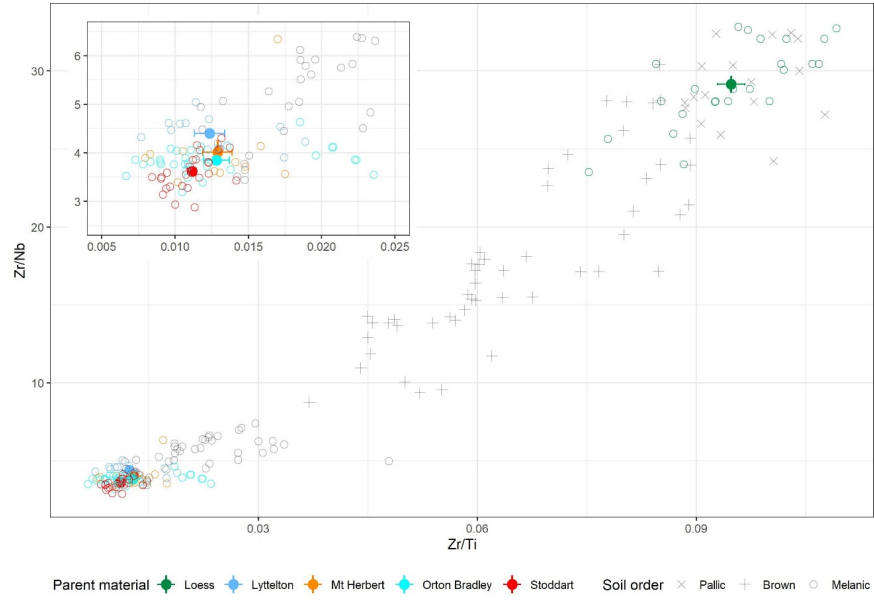


Figure S1: Plot of the parent material endmember and soil samples in the mixing space used in the Bayesian mixing modelling. The mixing space is well constrained and almost linear. The insert is a close-up of the space occupied by the volcanic rock endmembers.



Call: `varpart(Y = dat_AB, X = ~PET * bottom + MAT * bottom + MAP * bottom, ~propBasalt, data = meta_AB)`

Explanatory tables:

X1: `~PET * bottom + MAT * bottom + MAP * bottom`

X2: `~propBasalt`

No. of explanatory tables: 2

Total variation (SS): 581.1

Variance: 11.175

No. of observations: 53

Partition table:

	Df	R.squared	Adj.R.squared	Testable
[a+b] = X1	7	0.47713	0.39579	TRUE
[b+c] = X2	1	0.63175	0.62453	TRUE
[a+b+c] = X1+X2	8	0.75473	0.71014	TRUE
Individual fractions				
[a] = X1 X2	7		0.08561	TRUE
[b]	0		0.31019	FALSE
[c] = X2 X1	1		0.31435	TRUE
[d] = Residuals			0.28986	FALSE

Figure S2: Results of the variation partitioning. Shown is the graphical output indicating exclusive and shared partitions and the model summary that also indicates the variation assigned to the explanatory variables if the spatial correlation between climate and parent material had not been removed.

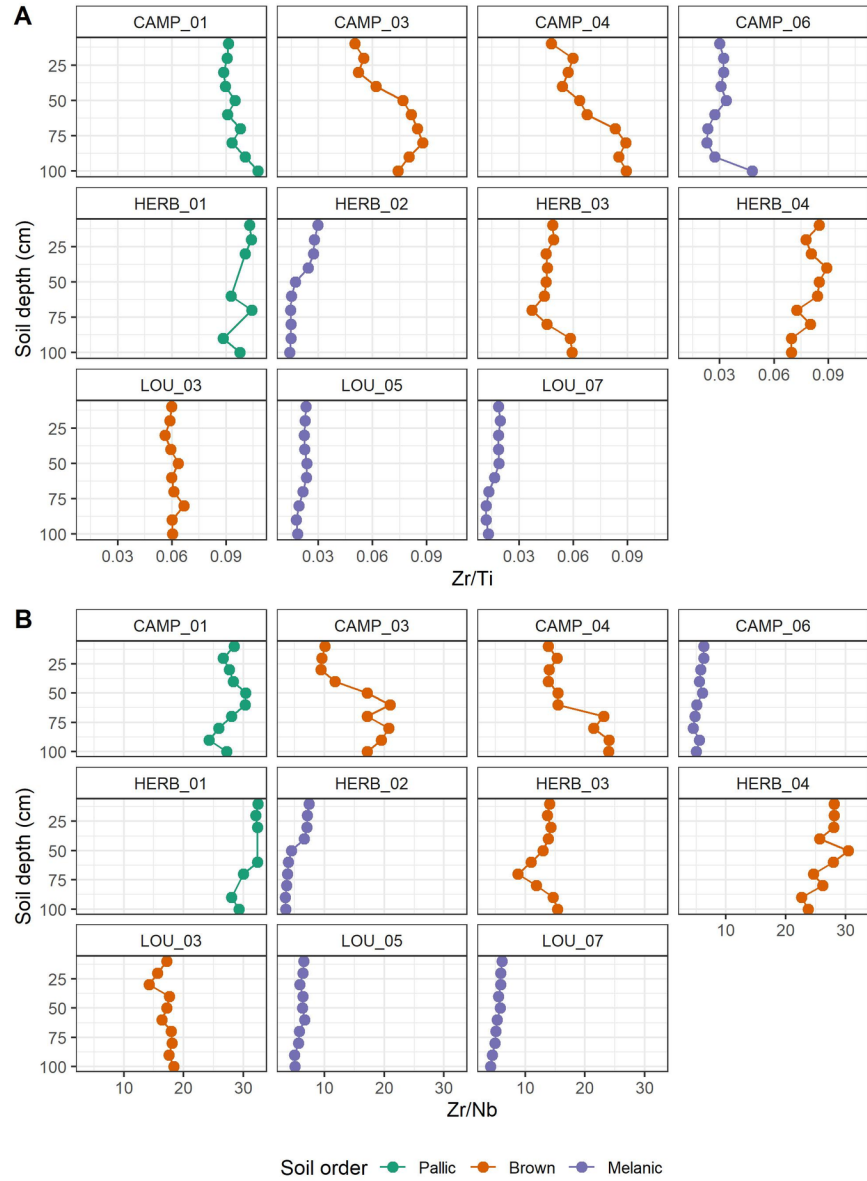


Figure S3: Ratios of immobile elements with depth across all soil sites, coloured by soil order. A) Zr/Ti, B) Zr/Nb. Note the variability in Pallid and Melanic soils, either indicating variability with a parent material group or non-conservative behaviour of some elements.

1 **Quantifying the Importance of Soil Forming Factors Using Multivariate Soil Data at**
2 **Landscape Scale**

3 **A. Eger¹, N. Koele², T. Caspari¹, M. Poggio^{3†}, K. Kumar³, and O. R. Burge⁴**

4 ¹Manaaki Whenua – Landcare Research, Soils & Landscapes, Lincoln 7608, New Zealand

5 ²Manaaki Whenua – Landcare Research, Land Use & Ecosystems, Lincoln 7608, New Zealand

6 ³Manaaki Whenua – Landcare Research, Land Use & Ecosystems, Palmerston North 4474, New
7 Zealand

8 ⁴Manaaki Whenua – Landcare Research, Ecosystems & Conservation, Lincoln 7608, New
9 Zealand

10 Corresponding author: A. Eger (egera@landcareresearch.co.nz)

11 †current address: Helmholtz-Zentrum für Umweltforschung, Department of Soil System Science,
12 06120 Halle, Germany

13 **Key Points:**

- 14 • Quantifying the importance of different soil forming factors that change concomitantly at
15 landscape scale (climate, parent material)
- 16 • Utilizing soils of an altitude gradient combined with proximal soil sensing data,
17 multivariate statistics and Bayesian mixing modelling
- 18 • Parent material explains three times more soil data variation than climate despite being
19 frequently omitted in modern digital soil mapping
- 20 •

21 **Abstract**

22 The role of soil forming factors (time, parent material, climate, biota, topography) on soil
23 processes has commonly been studied using soil sequences where only one factor varies between
24 sites. However, when multiple factors change, it becomes difficult to partition the importance of
25 different soil forming factors for soil formation. We show for an altitudinal gradient how
26 proximal sensing (portable XRF, Fourier-Transform Infrared [FTIR]), multivariate statistics and
27 Bayesian mixing modelling can help to quantify the importance of two soil forming factors.
28 First, we confirmed the existing qualitative soil-landscape model of concomitant shifts in parent
29 material (greywacke loess to mafic volcanics) and climate (higher precipitation) with altitude,
30 leading to increases in pedogenic oxides, soil carbon, and soil Fe, while Si concentrations and pH
31 declined. Second, we applied a mixing model using immobile elements as parent material tracers
32 to quantify the parent material contribution in soils across our gradient. Third, we conducted a
33 variation analysis to determine how much variation in the soil FTIR spectra could be explained
34 by parent material and climate. Parent material alone explained 31% of the variation, climate
35 alone only 9%. However, if we had only considered climate as explanatory variable, it would
36 have accounted for almost half of the total variation (41%) because of the strong interaction
37 between climate and parent material, and therefore concealing the leading role of parent material.
38 Given that parent material is often omitted in modern digital soil mapping, our results emphasize
39 the importance of parent material as a predictor of spatial soil distribution.

40 **1 Introduction**

41 A soil at a given location is the result of the integrated effects of multiple soil-forming
42 processes. This is generally represented by the soil forming factor approach, where these
43 processes are represented by their controlling environmental factors: climate, parent
44 material/lithology, biota, and topography acting collectively over time to define the
45 characteristics of a soil (Jenny, 1941). More recently, this long-standing concept has been put
46 into a spatial context as SCORPAN (soil, climate, organisms, relief/topography, parent material,
47 age, space: relative spatial position), a framework that is widely used for modelling the spatial
48 distribution of soils in modern digital soil mapping (McBratney et al., 2003): quantitative or
49 qualitative spatial information representing the SCORPAN factors are used as covariates to
50 predict the spatial distribution of soil properties or classes using statistical and other modelling
51 methods (e.g., Heung et al., 2016; Ma et al., 2017; McBratney et al., 2003; Odgers et al., 2011;
52 Zhang et al., 2020).

53 To understand the individual roles of soil forming factors to drive soil developmental
54 trajectories and closely inter-related ecological processes, scientific focus has been on
55 experimental settings where all but one of the soil-forming factors can be kept near-constant by
56 substitution for location. Most common examples of such well-constrained systems are
57 chronosequences (only time/age varies between sites) (e.g., Crews et al., 1995; Dorji et al., 2009;
58 Eger et al., 2011; Maher et al., 2009; S.J. Richardson et al., 2004; Tonkin & Basher, 2001; S.
59 Turner et al., 2017; Wardle et al., 2004), climosequences (only climate varies) (e.g., O. A.
60 Chadwick et al., 2003; Dere et al., 2013; Dixon et al., 2016; Helfenstein et al., 2018; Riebe et al.,
61 2004; B. L. Turner et al., 2018; Webb et al., 1986), toposequences (only topography varies) (e.g.,
62 Agbenin & Tiessen, 1994; Araújo et al., 2004; K. D. Chadwick & Asner, 2020; Porder et al.,
63 2005; S.J. Richardson et al., 2008; Vitousek et al., 2003) or parent material sequences/paired

64 sites (e.g., Bazilevskaya et al., 2013; Hahm et al., 2014; Mage & Porder, 2013; Vitousek et al.,
65 2016). These sequences have been a very powerful tool to understand fundamental processes of
66 soil formation, biogeochemical cycling, and above and below-ground ecological change (e.g.,
67 rock/mineral weathering, soil nutrient cycles, plant succession/retrogression, soil microbiology).
68 While scientifically important, such model systems are naturally rare. Instead, most terrestrial
69 landscapes are much less constrained, such that multiple soil forming factors concomitantly
70 change with location. Understanding the drivers of soil formation in such ‘messy’ spatial
71 contexts and the formulation of empirically supported soil-landscape models is however vital for
72 modern soil mapping approaches, since they rely on covariates that are structurally meaningful to
73 predict soil characteristics at a given locale (Behrens & Viscarra Rossel, 2020; Meyer et al.,
74 2019).

75 In our study we present a methodological approach to quantitatively disentangle the
76 effect of two soil forming factors on a given soil pattern. Our approach takes advantage of the
77 recent progress in soil proximal sensing methods (Fourier-Transform Infrared spectroscopy
78 [FTIR], portable X-ray fluorescence [pXRF]) and their increasing applicability and accessibility
79 in soil science with respect to faster sample turnaround, and lower analytical costs compared to
80 conventional laboratory methods (Viscarra Rossel et al., 2011; Viscarra Rossel et al., 2010). Our
81 case study uses soils along an altitudinal gradient, which represents both a change in parent
82 material (from wind-blown sediment [loess from greywacke] to volcanic extrusive rocks), and in
83 climate (from soils with an annual water deficit to soils that receive precipitation in excess of the
84 potential evapotranspiration). Our study opens new opportunities for improving our
85 understanding of mechanistic drivers of soil variability at landscape-scale, and highlights the
86 relevance of parent material specifically, a factor that is often neglected in modern soil mapping
87 approaches.

88

89 **2 Materials and Methods**

90 Firstly, we use soil chemical and proximal sensing data (FTIR, pXRF) to confirm the
91 qualitative description of the dual climate and parent material gradients at the site. Secondly, we
92 perform a parent material mixing model and examine its consistency with the soil chemical
93 properties. Thirdly, we assess the relative contributions of climate and parent material using
94 variance partitioning, with the FTIR data to identify which of the two soil forming factors is
95 more important for soil formation across our altitudinal gradient. All data used in the analysis
96 and discussion can be found in the Supplementary material.

97 **2.1 Study area**

98 The study sites are located at the northern flanks of Banks Peninsula, South Island, New
99 Zealand (Figure 1). The peninsula was constructed by a series of volcanic eruptions between 11
100 to 5.8 My ago and reaches a maximum altitude of 919 m asl. The volcanic lithology relevant for
101 our study is dominated by alkaline volcanic rocks (hawaiite, basalt, tuff, conglomerates).
102 Overall, the mineralogy is dominated by plagioclase (andesine, labradorite), sometimes co-
103 dominant with clinopyroxene, and subdominant olivine and Fe-oxides, including Fe-Ti magnetite
104 (Sewell, 1988a, 1988b; Sewell et al., 1993). Partially superimposed over the volcanic rocks is
105 Late Quaternary wind-blown sediment (loess) that can reach up to 15 m depth at lower
106 elevations (Sewell et al., 1993). The source lithology of the local loess is quartzofeldspathic

107 Triassic greywacke sandstone that dominates the bedrock geology of the eastern side of the
108 Southern Alps. Erosion of these ranges in the Quaternary formed an extensive alluvial fan
109 (Canterbury Plains), now partially submerged, in association with braided-river systems, acting
110 as the loess source. The loess parent material is dominated by quartz, ~30% feldspars (albite, K-
111 feldspar), and <10% of each muscovite and chlorite (Trangmar & Whitton, pers. communication;
112 Jowett, 1995; Raeside, 1964). The loess cover in Banks Peninsula thins with altitude and
113 increasing slope gradient, and is virtually absent above elevations of 500-600 m in our study
114 area. Concomitantly with altitude, annual averages of precipitation (MAP), temperature (MAT)
115 and Penman evapotranspiration (PET) change from ~600 mm/12.4°C/820 mm at sea-level to
116 ~1300 mm/9.3°C/650 mm at 900 m asl (Andrew Tait, National Institute of Water and
117 Atmospheric Research [NIWA], pers. communication, 2015). This climatic regime imposes an
118 annual water deficit of over 200 mm per year at sea level (Leathwick et al., 2002; Ministry for
119 the Environment, 2002).

120

121 *Figure 1: The study sites are located in the South Island of New Zealand, in the northern part of*
122 *Banks Peninsula. Aerial imagery and digital elevation model supplied by Land Information New*
123 *Zealand under CC BY 4.0 ([https://data.linz.govt.nz/layer/105027-canterbury-banks-peninsula-](https://data.linz.govt.nz/layer/105027-canterbury-banks-peninsula-lidar-1m-dem-2018-2019/)*
124 *[lidar-1m-dem-2018-2019/](https://data.linz.govt.nz/layer/53519-canterbury-03m-rural-aerial-photos-2015-2016/); [https://data.linz.govt.nz/layer/53519-canterbury-03m-rural-aerial-](https://data.linz.govt.nz/layer/53519-canterbury-03m-rural-aerial-photos-2015-2016/)*
125 *[photos-2015-2016/](https://data.linz.govt.nz/layer/53519-canterbury-03m-rural-aerial-photos-2015-2016/)).*

126 The changes of parent material and climate are reflected in the soil pattern as observed in
127 the field (Griffiths, 1973; Manaaki Whenua - Landcare Research, 2020; Trangmar, 1986): Fine-
128 grained soils (<2 mm particle size, mainly silt) from loess, often with fragipans and redox
129 mottling, dominate at low elevations (typical soils: Immature/Argilic/Fragic Pallic Soil; New
130 Zealand Soil Classification – Hapludalfs, Haplustalfs, Haplustepts, Fragiudepts; Soil Taxonomy)
131 (Hewitt, 1993; Soil Survey Staff, 1999). As altitude and slope gradient increase, soils are formed
132 in mixed loess-volcanic rock colluvia that normally comprise at least 5% volcanic rock
133 fragments (typical soils: Melanic Brown Soil – mainly Dystrudepts, subdominant: Rocky Recent
134 Soil – Lithic Udorthents). With further altitude increase, soils derived from volcanic rocks
135 become dominant, containing variable proportions of rock fragments, clay and sand (typical:
136 Mafic Melanic Soil – mainly Lithic/Typic Hapludoll, co-dominant: Rocky Recent Soil – Lithic
137 Udorthents), depending on the nature of the soil-forming substrate (e.g., mobile slope deposits,

138 saprolite). A similar soil pattern has also been recognised for Otago Peninsula 300 km south
 139 (Leslie, 1973a, 1973b). Vegetation cover today is mainly pasture for low intensity sheep and
 140 cattle farming. Prior to anthropogenic landcover change podocarp-hardwood forests dominated
 141 the peninsula.

142 2.2 Data collection and soil analysis to confirm the altitudinal gradient

143 Soil data were collected from 11 soil sites across three transects (Figure 1). The transects
 144 were selected on the basis of reflecting the variability of the volcanic lithology, representing a
 145 larger spatial extent beyond a single catchment, and having landowner approval. The soils were
 146 described in the field and classified according to the New Zealand Soil Classification (Table 1).
 147 Climate data were based on the period 1981-2010; they were produced by first calculating the
 148 30-year statistics at climate station locations with available data, followed by interpolation of
 149 these statistics onto a 500 m spatial resolution grid (Andrew Tait, NIWA, pers. communication,
 150 2015). Topographic site data was derived from a 1 m resolution digital elevation model
 151 (<https://data.linz.govt.nz/layer/105027-canterbury-banks-peninsula-lidar-1m-dem-2018-2019/>).
 152 We targeted Pallic (loess parent material), Brown (mixed loess-volcanic parent material) and
 153 Melanic soils (volcanic parent material) as typical pedons for the elevation gradient. We choose
 154 soils that we could core to 1 m depth to allow for comparison of soil data across all soils and all
 155 corresponding depths. We avoided any soils that showed evidence of colluvial burying (e.g.,
 156 buried topsoils) or erosion (e.g., missing topsoil or weathered B horizon). We acknowledge that
 157 our sampling omits shallower soils on bedrock that can occur at any elevation in our study area,
 158 but particularly at higher elevations. The elapsed time since the start of soil formation will
 159 undoubtedly vary between sites across our transects given the parent material differences (e.g.,
 160 Late Quaternary loess, Holocene regolith) and variable erosion rates (and consequently different
 161 distributions of soil particle ages). By not selecting very shallow soils, which generally have
 162 shorter residence times than deeper soils, we avoid the most extreme temporal inconsistencies.
 163 We sampled all soils to 100 cm at 10 cm depth intervals.

164

165 *Table 1: Overview of the soil sites used in this study.*

Site	Latitude (°)	Longitude (°)	NZ Soil classification	Soil Taxonomy	Formation	Elevation (m asl)	Local slope (°)	MA T (°C)	MAP (mm)	PET (mm)
CAMP_01	43.6238	172.7851	Mottled Fragic Pallic	Fragiudepts	Lyttelton, covered by >1 m loess	83	22	12.3	635	810
CAMP_03	43.6295	172.7963	Typic Mafic Brown	Dystrudepts	Lyttelton	360	27	11.6	692	769
CAMP_04	43.6288	172.8002	Typic Mafic Brown	Dystrudepts	Lyttelton	383	9	11.7	694	776
CAMP_06	43.6342	172.7947	Typic Mafic Melanic	Typic Hapludolls	Mt Herbert	499	19	11.1	767	740
HERB_01	43.6436	172.7328	Typic Fragic Pallic	Fragiudepts	Stoddart, covered by >1 m loess	272	7	12.2	828	811
HERB_02	43.6627	172.7355	Typic Mafic Melanic	Typic Hapludolls	Stoddart	493	4	11.0	1266	746
HERB_03	43.6660	172.7361	Typic Mafic Brown	Dystrudepts	Stoddart	504	7	10.5	1300	717

HERB_04	- 43.661 4	172.7395	Typic Mafic Brown	Dystrudepts	Stoddart	462	23	11.0	1266	746
LOU_03	- 43.687 5	172.6929	Typic Mafic Brown	Dystrudepts	Lyttelton	279	20	11.0	1216	760
LOU_05	- 43.690 9	172.6910	Typic Mafic Melanic	Typic Hapludolls	Lyttelton	288	15	10.6	1214	738
LOU_07	- 43.688 2	172.7031	Typic Mafic Melanic	Typic Hapludolls	Orton Bradley	490	35	10.4	1240	723

166 Acid-oxalate extractable Fe, Al, Si (Feo, Alo, Sio) was determined after Blakemore et al.
 167 (1987). The acid-oxalate extraction (0.2M oxalate at pH 3; 4 hours shaking in the dark) is used to
 168 quantify Fe, Al and Si bound to non-/poorly crystalline secondary soil components, including
 169 organic matter-metal complexes. Fe in crystalline pedogenic oxides (Fed) was determined by
 170 dithionite-citrate (Blakemore et al., 1987; Holmgren, 1967). Concentrations in the extracts were
 171 measured using ICP-OES. Soil pH was determined at a 1:5 soil/water weight ratio after 16h
 172 equilibration; electrical conductivity (EC) was also measured at a 1:5 soil:water ratio, shaken for
 173 30 minutes, allowed to settle, and then measured with a temperature-compensated probe
 174 (Blakemore et al., 1987). Moisture factor (MF) expresses the difference in moisture between the
 175 air-dried sample and the 105°C oven-dried sample (Blakemore et al., 1987). MF has been used as
 176 a proxy for reactive surface area (Parfitt et al., 2001). Organic carbon and total nitrogen were
 177 analyzed using a LECO TruMac (LECO Corporation, St. Joseph, MO, USA). Phosphate
 178 retention (weight %) of the soil was measured after Saunders (1965), using a KH_2PO_4 solution
 179 (25 mg P per 5 g of soil). The PO_4 retention of the soil was calculated from the difference
 180 between the original P content of the solution and the concentration after shaking the sample for
 181 16 hours. Soil PO_4 retention is an indicator for reactive, pedogenic oxides and metal-organic
 182 complexes and usually correlates with acid-oxalate extractions of Fe, Al and Si (Saunders, 1965).
 183 Analytic results are reported on 105°C oven-dry basis and represent the <2 mm fraction.

184 Proximal sensing methods were applied to air-dried samples, ground and passed through
 185 a 2 mm sieve. We measured total Ca, Si, K, Ti, Zr, Nb, Al, Fe, and Mn using an Olympus Vanta
 186 C series portable XRF (pXRF) instrument (Olympus, Waltham, USA), in bench mode in the
 187 laboratory using the internal 'Geochem' element calibration provided by the manufacturer for
 188 converting raw spectra into element concentrations as. The instrument is fitted with a Rhodium
 189 anode operated at up to 40 KeV with separate beams for light and heavy elements. Prior to
 190 analysis, we checked for potential contamination of the pXRF measurement window and tested
 191 the instrument measurements against the manufacturer-provided Alloy 316 (stainless steel)
 192 calibration check coupon and the NIST standard 2711a. Each sample was measured in a plastic
 193 cup, covered by a protective polypropylene 4.0 μm -film. Exposure time was 60 seconds for each
 194 beam per sample and measurement uncertainties (1σ) were recorded for each element. Elemental
 195 concentrations are reported on 105°C oven-dry basis.

196 On the same samples we also measured the mid-infrared (MIR) spectra using a Fourier-
 197 Transform Infrared (FTIR) spectrophotometer (Tensor II HTS-XT FTIR by Bruker). The spectral
 198 range was reduced to the MIR range between 4000 and 600 cm^{-1} . Each sample was scanned in
 199 four replicates, then averaged to account for possible heterogeneity within the soil samples. The
 200 diffuse reflectance data were transformed into absorbance spectra (absorbance = log
 201 [1/reflectance]) prior to statistical analysis.

202 2.3 Assessment of FTIR data against the altitudinal gradient

203 Based on previous research (Guillou et al., 2015) we selected a range of wavenumbers of
204 the FTIR data that are particularly indicative of mineralogical differences. We used the following
205 wavenumber regions 3730–3610 cm^{-1} , 1950–1750 cm^{-1} , and 1230–630 cm^{-1} (Guillou et al.,
206 2015). We applied an unconstrained ordination technique (Nonmetric Multidimensional Scaling
207 [NMDS]) to the selected wavenumbers to reduce the dimensions of the multivariate data to two
208 dimensions for visualization and interpretation. The analysis was performed in R version 4.0.2
209 (R Core Team, 2020) with the ‘vegan’ package (Oksanen et al., 2019) on untransformed data and
210 with Euclidean distance to calculate the distance matrix of all samples used in the NMDS fitting
211 (Oksanen et al., 2019).

212 2.4 Parent material modelling using pXRF data

213 To quantify the proportion of the two parent materials (greywacke loess, volcanics) in
214 each sample, we used the Bayesian mixing model MixSIAR in R (R Core Team, 2020; Stock et
215 al., 2018). In contrast to a simple linear mixing model approach (e.g., $z = f_x b_x + f_y b_y$, $1 = f_x + f_y$;
216 where z is tracer in mixed substrate, b_x is tracer in endmember X, b_y is tracer in endmember Y, f_x
217 and f_y are the relative proportions of the endmembers X and Y), MixSIAR allows us to
218 incorporate the uncertainty derived from endmember variability and random effects (Stock et al.,
219 2018; Stock & Semmens, 2016a, 2016b). We used an uninformative prior and the error
220 structures ‘process’ and ‘residual’, which assumes that each sample consists of parent materials
221 that may be derived from different parts of the respective endmember distributions and that the
222 parent materials in each soil can be subject to unknown deviations from the endmember means.
223 As random effect we used the underlying geological formation at each soil site to account for the
224 variability of the volcanic rock geochemistry in our study area. As parent material tracers we
225 chose the ratios of Zr/Ti and Zr/Nb as measured by pXRF in the soils, their suitability as tracers
226 is discussed in detail further below. For the volcanic endmember, we used Zr, Ti and Nb data
227 from Sewell (1988b), as derived from individual samples of the four local geological volcanic
228 rock formations relevant for the individual soil sites (Lytelton Fm, number of samples (n) = 12;
229 Mt Herbert Fm, n = 11; Orton Bradley Fm, n = 31; Stoddart Fm, n = 26) (Sewell, 1988b; Sewell
230 et al., 1993). To define the loess endmember, we used data from pedogenic C horizons of 4 soils
231 classified as Pallic soils derived from loess, as stored in the New Zealand’s National Soil
232 database (soil IDs: SB09997, SB10001, SB10002, SB10004; [https://viewer-
233 nsdr.landcareresearch.co.nz/search](https://viewer-nsdr.landcareresearch.co.nz/search)). In addition, we used data from C horizons of a soil
234 comprising multiple buried loess sheets (Claremont soil; Childs & Searle, 1975). Since the
235 Claremont data set did not contain Nb values, we augmented it with the average of the Nb values
236 from the 4 loess soils in the National Soil Database ($\mu = 12.475$, $\sigma = 1.451$). All of the samples
237 representing loess endmembers come from within 150 km of our study area and received the
238 loess from the same system of braided rivers/alluvial fans as our study area. Total number of
239 endmember loess samples was 24. Three of our soil samples plotted outside the maximum ranges
240 of parent material samples for Zr/Ti or Zr/Nb. These were excluded from the mixing model.
241 Figure S1 shows the endmembers and soil samples in the mixing space. While pXRF data has
242 been previously used for parent material fingerprinting (Mancini et al., 2019), to our knowledge
243 this is the first time that such Bayesian model was used to determine parent material provenance
244 in soils.

245 2.4 Assessment of parent material and climate as soil forming factors using variation
246 partitioning

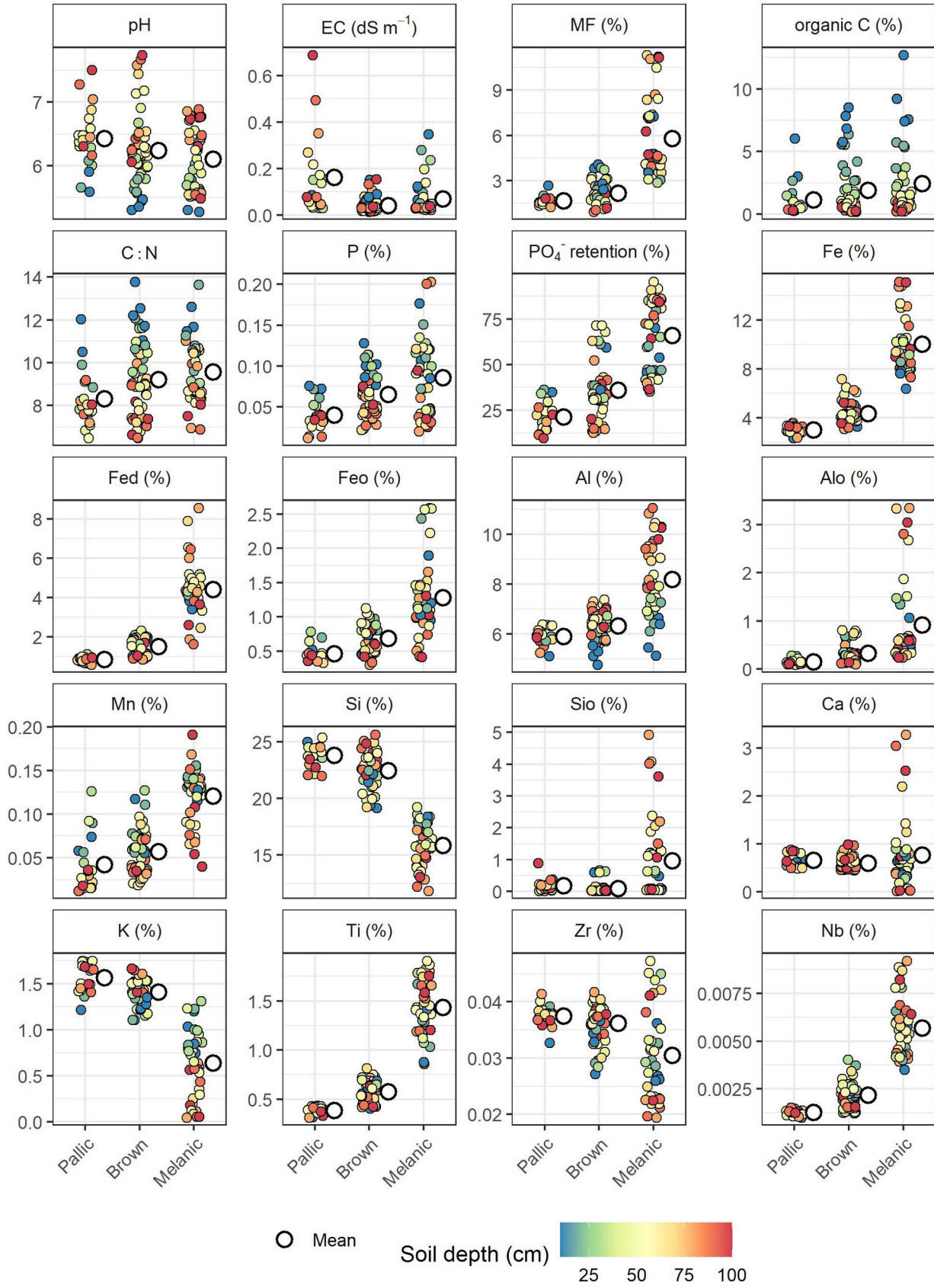
247 To compare the importance of parent material and climate across our transects in driving
248 the overall variation in the multivariate FTIR dataset, we also performed a variation partitioning
249 using the function *varpart* ('vegan' package). In the variation partitioning we used two sets of
250 explanatory variables: 1) the results of the parent material mixing model for each sample, and 2)
251 a combination of climate parameters for each sample site, where each of the climate parameters
252 (MAT, MAP, PET) interacts with soil depth (i.e., the effects of the parameters change with
253 depth). This approach allows us to partial out the correlation between both factors, parent
254 material and climate (i.e., volcanic rock influence on soils increases with altitude, while at the
255 same time MAT and PET decrease and MAP increases). The FTIR data as the response variable
256 was limited to the upper 50 cm to only include pedogenically altered parts of the soils (i.e., A
257 and B horizons).

258

259 **3 Results**

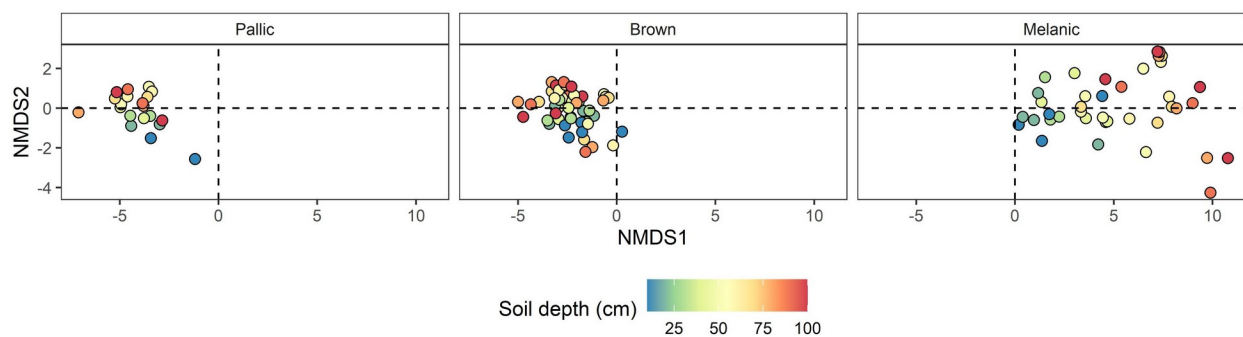
260 3.1 Soil chemistry and FTIR data of the altitudinal soil gradient

261 Most chemical soil properties (e.g., moisture factor, organic C, PO_4^- retention, various
262 fractions of Fe and Al, most of the total elements) confirm the intermediate chemical character of
263 Brown soils between Pallic and Melanic soils (Figure 2). Some variables show a particularly
264 strong contrast between soils derived from loess and volcanic parent material as represented by
265 Pallic and Melanic soils: higher concentrations of Fe, Al, Mn and Ti occur in Melanic soils,
266 whereas Si and K show higher concentrations in Pallic soils. Melanic soils show a characteristic
267 increase in K concentrations of K towards the surface. Ca concentrations in Melanic soils are, on
268 average, indifferent to those of Pallic or Brown soils. Soil pH values are on average slightly
269 lower in Melanic soils. Crystalline and non-crystalline pedogenic oxides, organic carbon and
270 moisture factor are lowest in Pallic soils and increase towards Brown and Melanic soils.



272 *Figure 2: Summary of the selected soil chemical properties. The data is summarised by the mean*
 273 *of each soil order, offset to the right of the raw data.*

274 The FTIR data in ordination space across the three main soils show a general drift across
 275 the x-axis values (NMDS1), in the order of Pallic soils < Brown soils < Melanic soils (Figure 3).
 276 Towards the surface, Melanic soils show smaller x-axis values, whereas the opposite but less
 277 clear trend seems to apply to Pallic and Brown soils. Overall, this results in an increasing
 278 convergence of the three soil orders towards the center of the ordination as soil depth becomes
 279 shallower. This increasing similarity of shallow samples is also corroborated by the chemistry
 280 data that shows lower absolute differences between the three soil orders as depth becomes
 281 shallower, particularly for the Melanic – Pallic/Brown comparison (Figure 2). Across both
 282 ordination axes Melanic soils show the largest variation compared to Pallic and Brown soils
 283 (Figure 3), a pattern that is also reflected in the variability of chemical properties, including those
 284 of our tracer elements (Ti, Zr, Nb) (Figure 2).

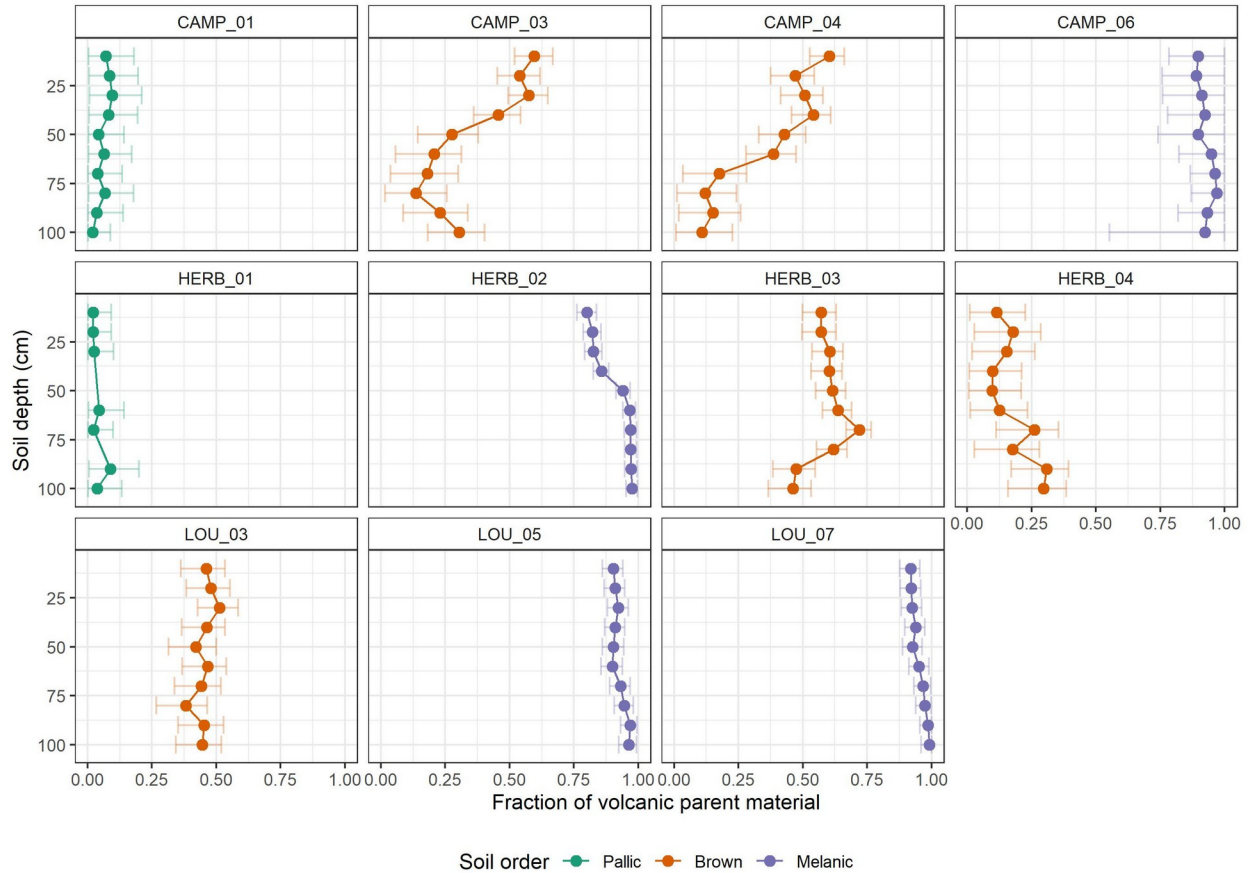


285

286 *Figure 3: NMDS ordination of the selected FTIR wavenumbers with indication of soil depth*
 287 *(base of sample), by soil order. Each soil order was plotted separately for better readability; the*
 288 *ordination space for all three panels is identical.*

289 3.2 Parent material modelling

290 The Bayesian mixing model results agree with the expected dominance of loess parent
 291 material in Pallic soils and that of volcanics in Melanic soils. Figure 4 shows the proportions of
 292 volcanic parent material across the depths of the soils. While the 95% confidence intervals are
 293 generally larger for Brown soils, these soils still form a distinct group in between the two
 294 endmember soil groups. In the soils CAMP_03 and 04, volcanic-dominated substrate is placed
 295 over more loess-dominated material, while the opposite case is indicated for HERB_04, and an
 296 even more complex deposition history is recorded for HERB_03. In contrast, LOU_03 shows a
 297 more monotonous depth relationship of the volcanic contribution.



298

299 *Figure 4: Mixing proportions with soil depth. Shown are medians and 95% confidence intervals*
 300 *of the fractions of volcanic parent material contribution to each depth increment.*

301 3.3 Parent material and climate as soil forming factors

302 The results of the variation partitioning (Figure S2) show that parent material alone
 303 accounts for 31% of the variation in the FTIR data, equal to the shared amount explained by
 304 parent material and climate. The shared amount reflects the spatial correlation of parent material
 305 and climate across our gradient. Only 9% of variation could be assigned to climate alone, while
 306 29% of total variation is explained by unknown variables (residuals). Without partitioning out
 307 the correlation between climate and parent material, climate would account for almost 40% of
 308 the total variation, whereas parent material would reach 62%.

309 4 Discussion

310 Through a combination of soil spectral data, Bayesian mixing modelling and multivariate
 311 statistics we were able to quantify the effect of the two spatially correlated soil forming factors,
 312 parent material and climate, on soil formation. Our results indicate the dominance of parent
 313 material over climate as controlling factor in soil formation across our altitudinal gradient.

314 4.1 Confirmation of the existing soil-landscape relationship

315 Initially we confirmed the consistency of the soil chemical and spectral data with the
 316 observed soil morphology and classification that formed the basis for the existing soil-landscape

317 model. The soil data confirms the intermediate chemical character of Brown soils between the
318 loess-derived, low elevation Pallic and volcanics-derived, high elevation Melanic soils (Figures 2
319 and 3). This is consistent with the existing understanding that the Brown soil characteristics are
320 both the result of parent material mixing (loess, volcanics) and mid-elevation climate. The
321 particularly strong contrast between soils derived from loess (Pallic) and volcanic parent material
322 (Melanic) in many elements reflects the strong imprint of mineralogy. Olivine, pyroxene, and Fe-
323 Ti oxides (and their weathering products) as typical minerals in the volcanic rock result in the
324 high concentrations of Fe, Al, Mn and Ti in Melanic, whereas the quartz and K-feldspar
325 components of in loess are behind the high Si and K concentrations in Pallic soils. The
326 increasing concentrations of K towards the surface in Melanic soils is likely indicative of plant
327 uplift (Jobbagy & Jackson, 2004) resulting in similar topsoil values across all soils despite the
328 differences of K concentrations in the parent material. The overall increasing similarity of the
329 shallow soil increments in all soils as indicated but the ordination of the FTIR data (Figure 3) is
330 likely a consequence of the similar pastoral land use across all sites. Albeit not directly measured
331 by us, from the mineral assemblage and the large Fe concentrations we would also expect to see
332 a much larger concentration of Mg as derived from olivine in Melanic soils. Surprisingly, Ca
333 concentrations are on average indifferent between soil orders. This may indicate that the general
334 higher abundance of Ca-rich plagioclase feldspars in volcanic parent material as compared to
335 albite/orthoclase-rich loess is not replicated in our soils despite Ca-rich plagioclase being
336 consistently listed as the main mineral of the local volcanic rocks in the extensive dataset ($n >$
337 200) by Sewell (1988b). Therefore, we think it is more likely that higher weathering and
338 leaching rates of base metals under a wetter climate at higher elevations has depleted Ca in most
339 Melanic soils. This is supported by the lower soil pH values in Melanic soils, which indicates
340 that the increased proton-supply driven by higher precipitation has more than compensated for
341 the initially larger buffer capacity derived from basic volcanic parent material in Melanic soils in
342 comparison to more felsic but drier loess soils. In addition, weathering rates of Ca- and Mg-rich
343 feldspars and other silicates found in volcanic parent material are higher than those of Na- or K-
344 feldspars and quartz that dominate the loess mineralogy given their higher solubility constants
345 (e.g., thermodynamic databases used by geochemical transport models; Parkhurst & Appelo,
346 2013; Steefel et al., 2015). Similarly, higher concentrations of crystalline and non-crystalline
347 pedogenic oxides in Melanic soils is likely to be a result of a wetter climate but also more easily
348 weatherable primary minerals releasing Fe, Al, and Si at higher rates, even despite total Si
349 content is much lower in Melanic soils. Given that organic carbon and moisture factor are tightly
350 linked to pedogenic oxides (e.g., Kirsten et al., 2021; Kleber et al., 2005; McNally et al., 2017;
351 Mikutta et al., 2006; Wiesmeier et al., 2019), their concomitant increase in Melanic soils is
352 unsurprising. Overall, we interpret the increased variability in in chemical properties and FTIR
353 ordination in Melanic soils (Figures 2 and 3) as an indicator for more advanced pedogenic
354 alterations than in the other soil orders, including secondary mineral formation (e.g., pedogenic
355 oxides), organic matter accumulation, and weathering and leaching (e.g., dilution/residual
356 enrichment of chemical index elements), causing increased horizontal differentiation within the
357 Melanic soils as a combination of higher mineral weathering rates and a wetter climate at higher
358 altitude.

359 In summary, the combined chemical and spectral datasets are consistent with expected
360 climate and parent material changes originally based on qualitative, soil morphological
361 assessments. To disentangle the contribution of climate and parent material as a control of this
362 pattern, we quantified the parent material contribution to each sample.

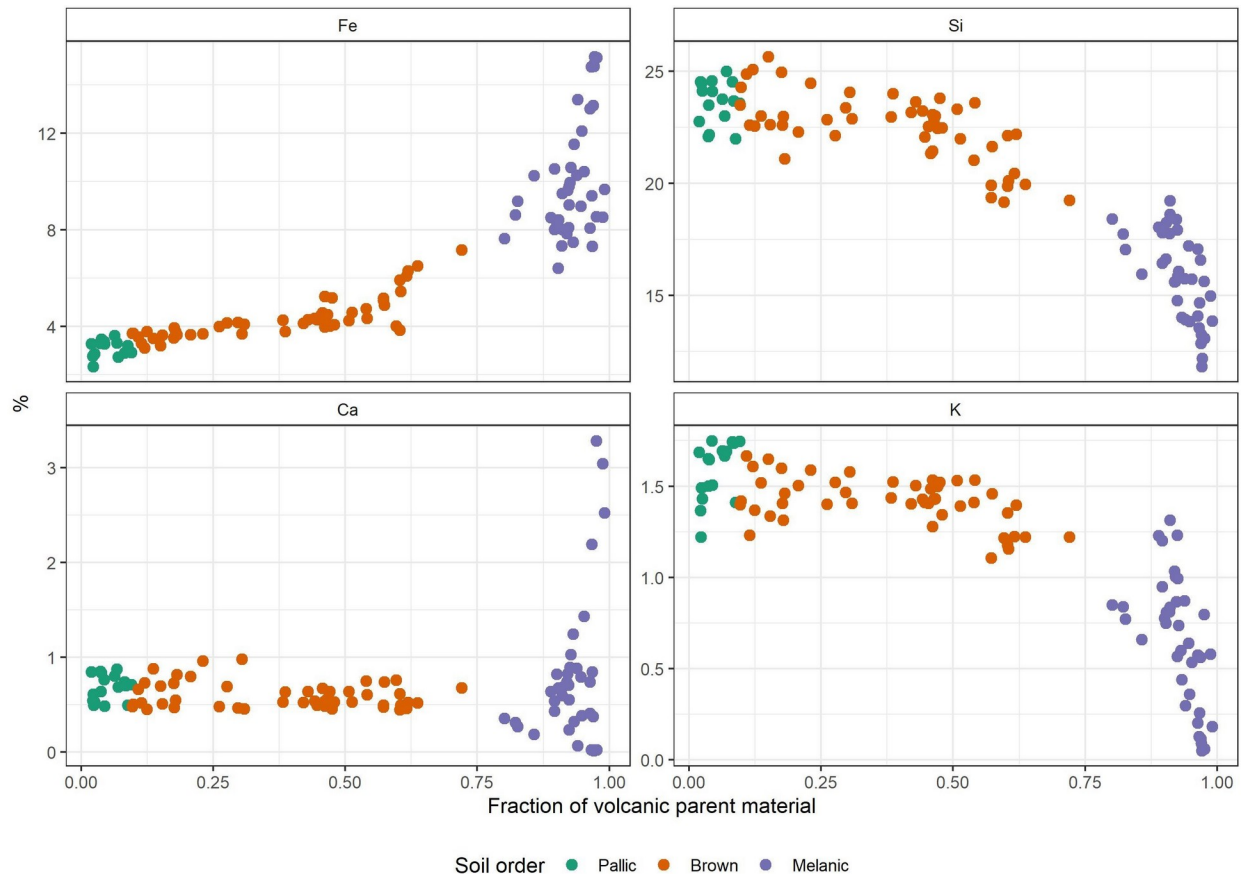
363 4.2 Soil parent material modelling using immobile elements and Bayesian mixing model

364 Before performing the mixing model we evaluated the assumption that Zr, Ti and Nb are
365 appropriate tracers for parent material. Zr, Ti and Nb are all elements that show minimal
366 chemical reactivity and mobility in soils because of low solubility (valence states of +4 and +5).
367 They have been widely used in pedology and geochemistry as conservative tracer for
368 quantitative mass balance calculations and geochemical source partitioning (e.g., Brantley &
369 White, 2009; O. A. Chadwick et al., 1990; O. A. Chadwick et al., 1999; Egli & Fitze, 2000;
370 Ferrier et al., 2011; Muhs et al., 2010; Riebe et al., 2003; White et al., 1998; Yoo et al., 2007).
371 We assume that the ratios of these elements in our soils only change due to parent material
372 changes but are irresponsive to chemical weathering. This is a simplification since variability
373 within a parent material group, and unknown external inputs to the soil can also affect these
374 ratios (e.g., Kurtz et al., 2000; Oeser et al., 2018). In addition, there is evidence that even low-
375 solubility elements can get mobilized under certain conditions (e.g., Cornu et al., 1999; Du et al.,
376 2012; Hodson, 2002). To test for immobility in natural conditions, the suspected immobile
377 elements are usually compared with each other to identify the most residually enriched elements
378 in the most chemically altered samples (e.g., Kurtz et al., 2000; Oeser et al., 2018). However,
379 this is not definitive evidence that an identified most enriched element is indeed immobile, rather
380 that it may be the least mobile elements out of all measured elements.

381 Figure S3 shows Zr plotted against Ti and Nb in each soil with depth. Even Pallic and
382 Melanic soils that we initially assumed to be either derived from loess or volcanic parent
383 material, respectively, show some variability. The data from HERB_02 even indicates that
384 compared to Zr, Nb and Ti are increasingly leached from the upper 40 cm of the profile.
385 However, we have confidence in using the selected element ratios as tracers in our mixing model
386 for two reasons. Firstly, within the context of the complete mixing space of soils and parent
387 material endmembers (Figure S1), the variability of the ratios of immobile elements in Pallic and
388 Melanic soils has limited impact. The variability in the Pallic soils is entirely contained within
389 the ranges of Zr/Nb, and Zr/Ti in the endmember samples of the loess. For the Melanic soils,
390 samples are mostly contained within the linear mixing space and, while a preferential leaching of
391 Nb and Ti compared to Zr could be behind the shift of some samples of Melanic soils beneath
392 the linear relationship, potentially overestimating the loess component in soils by interpreting
393 larger Zr/Ti and Zr/Nb ratios due to weathering as parent material signals instead. The alternative
394 explanation would be that even soils that we assume to be derived from volcanic parent material
395 still have a low loess input (e.g., HERB_02). Secondly, Figure S1 shows that the variability of
396 immobile element ratios within each parent material endmember is small in comparison to the
397 differences between the loess and volcanics. In addition, Figure S1 indicates that there is little
398 evidence for an additional parent material endmember in the soils, given the near-linear
399 relationship between endmembers and soil samples.

400 The results of the mixing model confirm the expected dominance of loess parent material
401 in Pallic soils, that of volcanics in Melanic soils and the mixed parent material in Brown soils
402 (Figure 4). Overall, the results of the mixing model are consistent with other indicators of parent
403 material provenance with minor modification by climate (Figure 5): total Si content decreases
404 with increasing proportion of volcanics in each sample as loess-derived quartz content declines.
405 The opposite pattern applies to total Fe as Fe-bearing minerals increase with increased volcanic
406 input. Concerning more mobile base metals, total K content decreases with increasing proportion
407 of volcanics as loess-derived K-feldspar content declines but likely also due to increased

408 leaching in volcanic-dominated soils limited to higher altitudes under greater precipitation.
 409 Increased leaching at higher altitude is also likely behind the lack of a correlation of total Ca
 410 with parent material provenance effectively offsetting the larger Ca content of unweathered
 411 volcanic parent material, except for deeper subsoil increments as discussed above. While an
 412 overestimation of the loess parent material may occur in our model, the effect appears to be
 413 limited given the consistent relationships with the chemical proxies. HERB_02, which showed
 414 the strongest indication that Ti and Nb is mobilized in the soil compared to Zr (Figure S3), is still
 415 overwhelmingly dominated by volcanic parent material.



416
 417 *Figure 5: Results of the parent material mixing model (x-axis) plotted against main element*
 418 *concentrations (y-axis). Note the panel headings for the different elements. Modelled parent*
 419 *material proportions of the volcanic rock (1-x for loess) grouped by soil order are consistent*
 420 *with mineralogy and climate.*

421

422 4.3 Importance of parent material and climate as soil forming factors

423 The results from the variation partitioning indicate that parent material explains a much
 424 larger variation in the FTIR data than climate. Given the distinct mineralogical differences
 425 between felsic greywacke loess and mafic volcanics, this result is plausible. However, our
 426 observations have practical relevance for digital soil mapping. Many digital soil mapping
 427 approaches focus on quantitative, spatial covariates. Across the set of soil forming factors,
 428 climate, vegetation and topography are generally available in this quantitative form, given the

429 advances in digital elevation models, lidar, remote sensing, and spatial modelling of climate
430 parameters. In contrast, spatial information on parent material is mostly available only as
431 categorical variables (e.g., lithology classes of geological maps), or do not exist at the required
432 mapping scales. Therefore, it is unsurprising that parent material has often been omitted in the
433 sets of covariates used for digital soil mapping (Gray et al., 2016; Grunwald, 2009; Lamichhane
434 et al., 2019). In our case study, if we only used climate parameters to explain the FTIR data, we
435 would 1) potentially misidentify climate as the major driver of variability across our altitude
436 gradient and miss the significance of parent material for the soils, and 2) lose the large
437 explanatory power of parent material in modelling/predicting the soil properties data.

438 Our example emphasizes the relevance of parent material characterization for explaining
439 soil properties in a landscape context. Our results suggest that a consideration of parent material
440 can not only aid the predictive capability of statistical and otherwise models, but also enhance
441 the utility of such models for understanding the mechanistic drivers of soil properties within a
442 spatial context (see also Gray et al., 2016). We therefore advocate for more efforts towards
443 developing quantitative soil parent material data sets adequate for the scale and environmental
444 conditions of the mapping space, and encourage their use in digital soil mapping (e.g., Bonfatti et
445 al., 2020; Gray et al., 2016; Mancini et al., 2019).

446 **5 Conclusions**

447 We used an altitudinal soil gradient with concomitant changes of greywacke loess to
448 volcanic rock, and drier to wetter climate, to show how relatively inexpensive and rapid soil
449 spectral methods can help to separate the effects of parent material and climate in driving soil
450 properties. We used chemically conservative tracer elements combined with a Bayesian mixing
451 model to identify the parent material contribution in each sample and found that the results were
452 consistent with other soil chemical data. By partitioning out the spatial correlation between
453 climate and parent material using a variation analysis, we were able to statistically confirm that
454 parent material and not climate explains a larger part of the variation in our FTIR soil spectra.
455 We conclude that multivariate statistics, and mixing models coupled to soil spectroscopy are
456 useful tools to improve our understanding of landscape-scale drivers of soil variation even when
457 multiple factors change concomitantly. Our work emphasizes the role of parent material as an
458 important explanatory, but often neglected, variable in modern soil mapping.

459 **Acknowledgments, Samples, and Data**

460 The raw data for this publication and R code used in the data analyses are available in the
461 supplementary material and under [https://datastore.landcareresearch.co.nz/dataset/jgr-](https://datastore.landcareresearch.co.nz/dataset/jgr-soilformingfactors)
462 [soilformingfactors](https://datastore.landcareresearch.co.nz/dataset/jgr-soilformingfactors). We thank the landowners for access to the sampling sites. The work was
463 partially funded by the Ministry of Business and Innovation through the Strategic Science
464 Investment Fund to Manaaki Whenua-Landcare Research (MWLR). The conception of the work
465 benefitted from a soil survey contract awarded to MWLR by Environment Canterbury and
466 unpublished reports by B. B. Trangmar and J. S. Whitton of the former NZ Soil Bureau. We
467 thank Ngaire Forster and her staff at MWLR's soil chemistry laboratory for the soil analysis,
468 Hugh Smith and Pierre Roudier for discussions of some aspects of this work, and Yuxin Ma for
469 reviewing an earlier version of this work.

470 **References**

- 471 Agbenin, J. O., & Tiessen, H. (1994). Phosphorus transformations in a toposequence of lithosols and cambisols from
 472 semi-arid northeastern Brazil. *Geoderma*, 62(4), 345-362. [http://www.sciencedirect.com/science/article/pii/](http://www.sciencedirect.com/science/article/pii/S0016706194900981)
 473 [0016706194900981](http://www.sciencedirect.com/science/article/pii/S0016706194900981)
- 474 Araújo, M. S. B., Schaefer, C. E. R., & Sampaio, E. V. S. B. (2004). Soil phosphorus fractions from toposequences
 475 of semi-arid Latosols and Luvisols in northeastern Brazil. *Geoderma*, 119(3-4), 309-321.
 476 <http://www.sciencedirect.com/science/article/pii/S0016706103002702>
- 477 Bazilevskaya, E., Lebedeva, M., Pavich, M., Rother, G., Parkinson, D. Y., Cole, D., & Brantley, S. L. (2013). Where
 478 fast weathering creates thin regolith and slow weathering creates thick regolith. *Earth Surface Processes*
 479 *and Landforms*, 38(8), 847-858. <https://onlinelibrary.wiley.com/doi/abs/10.1002/esp.3369>
- 480 Behrens, T., & Viscarra Rossel, R. A. (2020). On the interpretability of predictors in spatial data science: the
 481 information horizon. *Scientific Reports*, 10(1), 16737. <https://doi.org/10.1038/s41598-020-73773-y>
- 482 Blakemore, L. C., Searle, B. K., & Daly, B. K. N. (1987). Methods for chemical analysis of soils. *Soil Bureau*
 483 *Scientific Report*, 80.
- 484 Bonfatti, B. R., Demattê, J. A. M., Marques, K. P. P., Poppiel, R. R., Rizzo, R., Mendes, W. d. S., et al. (2020).
 485 Digital mapping of soil parent material in a heterogeneous tropical area. *Geomorphology*, 367, 107305.
 486 <https://www.sciencedirect.com/science/article/pii/S0169555X20302774>
- 487 Brantley, S. L., & White, A. F. (2009). Approaches to Modeling Weathered Regolith. *Reviews in Mineralogy and*
 488 *Geochemistry*, 70(1), 435-484. <https://doi.org/10.2138/rmg.2009.70.10>
- 489 Chadwick, K. D., & Asner, G. P. (2020). Geomorphic transience moderates topographic controls on tropical canopy
 490 foliar traits. *Ecology Letters*, 23(8), 1276-1286. <https://onlinelibrary.wiley.com/doi/abs/10.1111/ele.13531>
- 491 Chadwick, O. A., Brimhall, G. H., & Hendricks, D. M. (1990). From a black to a gray box -- a mass balance
 492 interpretation of pedogenesis. *Geomorphology*, 3(3-4), 369-390.
- 493 Chadwick, O. A., Derry, L., Vitousek, P., Huebert, B., & Hedin, L. (1999). Changing sources of nutrients during
 494 four million years of ecosystem development. *Nature*, 397(6719), 491-497.
- 495 Chadwick, O. A., Gavenda, R. T., Kelly, E. F., Ziegler, K., Olson, C. G., Elliott, W. C., & Hendricks, D. M. (2003).
 496 The impact of climate on the biogeochemical functioning of volcanic soils. *Chemical Geology*, 202(3-4),
 497 195-223.
- 498 Childs, C. W., & Searle, P. L. (1975). *Element distributions in loess columns at Claremont, Table Flat and Stewarts*
 499 *Claim, New Zealand*. Retrieved from <http://doi.org/10.7931/DL1-SBSR-20>
- 500 Cornu, S., Lucas, Y., Lebon, E., Ambrosi, J. P., Luizão, F., Rouiller, J., et al. (1999). Evidence of titanium mobility
 501 in soil profiles, Manaus, central Amazonia. *Geoderma*, 91(3-4), 281-295.
- 502 Crews, T. E., Kitayama, K., Fownes, J. H., Riley, R. H., Herbert, D. A., Mueller-Dombois, D., & Vitousek, P. M.
 503 (1995). Changes in Soil Phosphorus Fractions and Ecosystem Dynamics across a Long Chronosequence in
 504 Hawaii. *Ecology*, 76(5), 1407-1424.
- 505 Dere, A. L., White, T. S., April, R. H., Reynolds, B., Miller, T. E., Knapp, E. P., et al. (2013). Climate dependence
 506 of feldspar weathering in shale soils along a latitudinal gradient. *Geochimica et Cosmochimica Acta*, 122,
 507 101-126. <https://doi.org/10.1016/j.gca.2013.08.001>
- 508 Dixon, J. L., Chadwick, O. A., & Vitousek, P. M. (2016). Climate-driven thresholds for chemical weathering in
 509 postglacial soils of New Zealand. *Journal of Geophysical Research: Earth Surface*, 121(9), 1619-1634.
 510 <https://agupubs.onlinelibrary.wiley.com/doi/abs/10.1002/2016JF003864>
- 511 Dorji, T., Caspari, T., Bäumler, R., Veldkamp, A., Jongmans, A., Tshering, K., et al. (2009). Soil development on
 512 Late Quaternary river terraces in a high montane valley in Bhutan, Eastern Himalayas. *CATENA*, 78(1), 48-
 513 59.
- 514 Du, X., Rate, A. W., & Gee, M. A. M. (2012). Redistribution and mobilization of titanium, zirconium and thorium
 515 in an intensely weathered lateritic profile in Western Australia. *Chemical Geology*, 330-331, 101-115.
 516 <http://www.sciencedirect.com/science/article/pii/S0009254112003890>
- 517 Eger, A., Almond, P. C., & Condon, L. M. (2011). Pedogenesis, soil mass balance, phosphorus dynamics and
 518 vegetation communities across a Holocene soil chronosequence in a super-humid climate, South Westland,
 519 New Zealand. *Geoderma*, 163(3-4), 185-196.
 520 <http://www.sciencedirect.com/science/article/pii/S0016706111000875>
- 521 Egli, M., & Fitze, P. (2000). Formulation of pedologic mass balance based on immobile elements: a revision. *Soil*
 522 *Science*, 165(5), 437-443.

- 523 Ferrier, K. L., Kirchner, J. W., & Finkel, R. C. (2011). Estimating millennial-scale rates of dust incorporation into
 524 eroding hillslope regolith using cosmogenic nuclides and immobile weathering tracers. *J. Geophys. Res.*,
 525 *116*(F3), F03022. <http://dx.doi.org/10.1029/2011JF001991>
- 526 Gray, J. M., Bishop, T. F. A., & Wilford, J. R. (2016). Lithology and soil relationships for soil modelling and
 527 mapping. *CATENA*, *147*, 429-440. <https://www.sciencedirect.com/science/article/pii/S0341816216303046>
- 528 Griffiths, E. (1973). Loess of Banks Peninsula. *New Zealand Journal of Geology and Geophysics*, *16*(3), 657-675.
 529 <https://doi.org/10.1080/00288306.1973.10431388>
- 530 Grunwald, S. (2009). Multi-criteria characterization of recent digital soil mapping and modeling approaches.
 531 *Geoderma*, *152*(3), 195-207. <https://www.sciencedirect.com/science/article/pii/S0016706109001827>
- 532 Guillou, F. L., Wetterlind, W., Viscarra Rossel, R. A., Hicks, W., Grundy, M., & Tuomi, S. (2015). How does
 533 grinding affect the mid-infrared spectra of soil and their multivariate calibrations to texture and organic
 534 carbon? *Soil Research*, *53*(8), 913-921. <https://www.publish.csiro.au/paper/SR15019>
- 535 Hahm, W. J., Riebe, C. S., Lukens, C. E., & Araki, S. (2014). Bedrock composition regulates mountain ecosystems
 536 and landscape evolution. *Proceedings of the National Academy of Sciences*, *111*(9), 3338-3343.
 537 <http://www.pnas.org/content/111/9/3338.abstract>
- 538 Helfenstein, J., Tamburini, F., von Sperber, C., Massey, M. S., Pistocchi, C., Chadwick, O. A., et al. (2018).
 539 Combining spectroscopic and isotopic techniques gives a dynamic view of phosphorus cycling in soil.
 540 *Nature Communications*, *9*(1), 3226. <https://doi.org/10.1038/s41467-018-05731-2>
- 541 Heung, B., Ho, H. C., Zhang, J., Knudby, A., Bulmer, C. E., & Schmidt, M. G. (2016). An overview and
 542 comparison of machine-learning techniques for classification purposes in digital soil mapping. *Geoderma*,
 543 *265*, 62-77. <https://www.sciencedirect.com/science/article/pii/S0016706115301300>
- 544 Hewitt, A. E. (1993). New Zealand soil classification. *Landcare Research science series*, *1*, 1-133.
- 545 Hodson, M. E. (2002). Experimental evidence for mobility of Zr and other trace elements in soils. *Geochimica et*
 546 *Cosmochimica Acta*, *66*(5), 819-828.
- 547 Holmgren, G. G. S. (1967). A Rapid Citrate-Dithionite Extractable Iron Procedure. *Soil Science Society of America*
 548 *Journal*, *31*(2), 210-211.
 549 <https://access.onlinelibrary.wiley.com/doi/abs/10.2136/sssaj1967.03615995003100020020x>
- 550 Jenny, H. (1941). *Factors of soil formation: a system of quantitative pedology*. New York: Mc-Graw-Hill.
- 551 Jobbagy, E. G., & Jackson, R. B. (2004). The uplift of soil nutrients by plants: biogeochemical consequences across
 552 scales. *Ecology*, *85*(9), 2380-2389. <http://www.esajournals.org/doi/abs/10.1890/03-0245>
- 553 Jowett, T. W. D. (1995). *An Investigation of the Geotechnical properties of loess from Canterbury and*
 554 *Marlborough*. (MSc), University of Canterbury, Christchurch.
- 555 Kirsten, M., Mikutta, R., Vogel, C., Thompson, A., Mueller, C. W., Kimaro, D. N., et al. (2021). Iron oxides and
 556 aluminous clays selectively control soil carbon storage and stability in the humid tropics. *Scientific Reports*,
 557 *11*(1), 5076. <https://doi.org/10.1038/s41598-021-84777-7>
- 558 Kleber, M., Mikutta, R., Torn, M. S., & Jahn, R. (2005). Poorly crystalline mineral phases protect organic matter in
 559 acid subsoil horizons. *European Journal of Soil Science*, *56*(6), 717-725. <http://dx.doi.org/10.1111/j.1365-2389.2005.00706.x>
- 560 Kurtz, A. C., Derry, L. A., Chadwick, O. A., & Alfano, M. J. (2000). Refractory element mobility in volcanic soils.
 561 *Geology*, *28*(8), 683-686. <http://geology.geoscienceworld.org/cgi/content/abstract/28/8/683>
- 562 Lamichhane, S., Kumar, L., & Wilson, B. (2019). Digital soil mapping algorithms and covariates for soil organic
 563 carbon mapping and their implications: A review. *Geoderma*, *352*, 395-413.
 564 <https://www.sciencedirect.com/science/article/pii/S0016706119300540>
- 565 Leathwick, J. R., New Zealand. Ministry for the E., Manaaki Whenua-Landcare Research New Zealand, L., &
 566 Landcare Research New, Z. (2002). *Land environments of New Zealand = Nga taiao o Aotearoa : a*
 567 *technical guide*. Auckland: Ministry for the Environment.
- 568 Leslie, D. M. (1973a). Quaternary deposits and surfaces in a volcanic landscape on Otago Peninsula. *New Zealand*
 569 *Journal of Geology and Geophysics*, *16*(3), 557-566. <https://doi.org/10.1080/00288306.1973.10431378>
- 570 Leslie, D. M. (1973b). Relationship between soils and regolith in a volcanic landscape on Otago Peninsula. *New*
 571 *Zealand Journal of Geology and Geophysics*, *16*(3), 567-574.
 572 <https://doi.org/10.1080/00288306.1973.10431379>
- 573 Ma, Y., Minasny, B., & Wu, C. (2017). Mapping key soil properties to support agricultural production in Eastern
 574 China. *Geoderma Regional*, *10*, 144-153.
 575 <https://www.sciencedirect.com/science/article/pii/S2352009417300615>
- 576

- 577 Mage, S. M., & Porder, S. (2013). Parent Material and Topography Determine Soil Phosphorus Status in the
578 Luquillo Mountains of Puerto Rico. *Ecosystems*, 16(2), 284-294. journal article.
579 <http://dx.doi.org/10.1007/s10021-012-9612-5>
- 580 Maher, K., Steefel, C. I., White, A. F., & Stonestrom, D. A. (2009). The role of reaction affinity and secondary
581 minerals in regulating chemical weathering rates at the Santa Cruz Soil Chronosequence, California.
582 *Geochimica et Cosmochimica Acta*, 73(10), 2804-2831.
583 <http://www.sciencedirect.com/science/article/pii/S0016703709000775>
- 584 Manaaki Whenua - Landcare Research. (2020). *S-map - New Zealand's national digital soil map*. Retrieved from:
585 doi.org/10.7931/L1WC7
- 586 Mancini, M., Weindorf, D. C., Chakraborty, S., Silva, S. H. G., dos Santos Teixeira, A. F., Guilherme, L. R. G., &
587 Curi, N. (2019). Tracing tropical soil parent material analysis via portable X-ray fluorescence (pXRF)
588 spectrometry in Brazilian Cerrado. *Geoderma*, 337, 718-728.
589 <https://www.sciencedirect.com/science/article/pii/S0016706118316069>
- 590 McBratney, A. B., Mendonça Santos, M. L., & Minasny, B. (2003). On digital soil mapping. *Geoderma*, 117(1), 3-
591 52. <https://www.sciencedirect.com/science/article/pii/S0016706103002234>
- 592 McNally, S. R., Beare, M. H., Curtin, D., Meenken, E. D., Kelliher, F. M., Calvelo Pereira, R., et al. (2017). Soil
593 carbon sequestration potential of permanent pasture and continuous cropping soils in New Zealand. *Global*
594 *Change Biology*, 23(11), 4544-4555. <https://onlinelibrary.wiley.com/doi/abs/10.1111/gcb.13720>
- 595 Meyer, H., Reudenbach, C., Wöllauer, S., & Nauss, T. (2019). Importance of spatial predictor variable selection in
596 machine learning applications – Moving from data reproduction to spatial prediction. *Ecological*
597 *Modelling*, 411, 108815. <https://www.sciencedirect.com/science/article/pii/S0304380019303230>
- 598 Mikutta, R., Kleber, M., Torn, M. S., & Jahn, R. (2006). Stabilization of Soil Organic Matter: Association with
599 Minerals or Chemical Recalcitrance? *Biogeochemistry*, 77(1), 25-56. [https://doi.org/10.1007/s10533-005-](https://doi.org/10.1007/s10533-005-0712-6)
600 [0712-6](https://doi.org/10.1007/s10533-005-0712-6)
- 601 Ministry for the Environment. (2002). LENZ - Annual water deficit (Publication no.
602 <https://doi.org/10.7931/L1KM2>). from Ministry for the Environment
- 603 Muhs, D. R., Budahn, J., Avila, A., Skipp, G., Freeman, J., & Patterson, D. (2010). The role of African dust in the
604 formation of Quaternary soils on Mallorca, Spain and implications for the genesis of Red Mediterranean
605 soils. *Quaternary Science Reviews*, 29(19), 2518-2543.
606 <http://www.sciencedirect.com/science/article/pii/S0277379110001228>
- 607 Odgers, N. P., McBratney, A. B., & Minasny, B. (2011). Bottom-up digital soil mapping. II. Soil series classes.
608 *Geoderma*, 163(1), 30-37. <https://www.sciencedirect.com/science/article/pii/S0016706111000760>
- 609 Oeser, R. A., Stroncik, N., Moskwa, L.-M., Bernhard, N., Schaller, M., Canessa, R., et al. (2018). Chemistry and
610 microbiology of the Critical Zone along a steep climate and vegetation gradient in the Chilean Coastal
611 Cordillera. *CATENA*, 170, 183-203. <http://www.sciencedirect.com/science/article/pii/S034181621830225X>
- 612 Oksanen, J., Blanchet, F. G., Friendly, M., Kindt, R., Legendre, P., McGlinn, D., et al. (2019). vegan: Community
613 Ecology Package (Version R package version 2.5-6). Retrieved from
614 <https://CRAN.R-project.org/package=vegan>
- 615 Parfitt, R. L., Whitton, J. S., & Theng, B. K. G. (2001). Surface reactivity of A horizons towards polar compounds
616 estimated from water adsorption and water content. *Soil Research*, 39(5), 1105-1110.
617 <https://www.publish.csiro.au/paper/SR00059>
- 618 Parkhurst, D. L., & Appelo, C. A. J. (2013). *Description of input and examples for PHREEQC version 3 - A*
619 *computer program for speciation, batch-reaction, one-dimensional transport, and inverse geochemical*
620 *calculations*. Denver: U.S. Geological Survey.
- 621 Porder, S., Paytan, A., & Vitousek, P. M. (2005). Erosion and landscape development affect plant nutrient status in
622 the Hawaiian Islands. *Oecologia*, 142(3), 440-449. <https://doi.org/10.1007/s00442-004-1743-8>
- 623 R Core Team. (2020). R: A language and environment for statistical computing. Vienna: R Foundation for Statistical
624 Computing. Retrieved from <https://www.R-project.org/>
- 625 Raeside, J. D. (1964). Loess Deposits of the South Island, New Zealand, and Soils Formed on them. *New Zealand*
626 *Journal of Geology and Geophysics*, 7(4), 811-838. <https://doi.org/10.1080/00288306.1964.10428132>
- 627 Richardson, S. J., Allen, R. B., & Doherty, J. E. (2008). Shifts in leaf N:P ratio during resorption reflect soil P in
628 temperate rainforest. *Functional Ecology*, 22(4), 738-745. [http://dx.doi.org/10.1111/j.1365-](http://dx.doi.org/10.1111/j.1365-2435.2008.01426.x)
629 [2435.2008.01426.x](http://dx.doi.org/10.1111/j.1365-2435.2008.01426.x)
- 630 Richardson, S. J., Peltzer, D. A., Allen, R. B., McGlone, M. S., & Parfitt, R. L. (2004). Rapid development of
631 phosphorus limitation in temperate rainforest along the Franz Josef soil chronosequence. *Oecologia*,
632 139(2), 267-276. <https://doi.org/10.1007/s00442-004-1501-y>

- 633 Riebe, C. S., Kirchner, J. W., & Finkel, R. C. (2003). Long-term rates of chemical weathering and physical erosion
634 from cosmogenic nuclides and geochemical mass balance. *Geochimica et Cosmochimica Acta*, 67(22),
635 4411-4427.
- 636 Riebe, C. S., Kirchner, J. W., & Finkel, R. C. (2004). Erosional and climatic effects on long-term chemical
637 weathering rates in granitic landscapes spanning diverse climate regimes. *Earth and Planetary Science*
638 *Letters*, 224(3-4), 547-562. <https://doi.org/10.1016/j.epsl.2004.05.019>
- 639 Saunders, W. M. H. (1965). Phosphate retention by New Zealand soils and its relationship to free sesquioxides,
640 organic matter, and other soil properties. *New Zealand Journal of Agricultural Research*, 8(1), 30-57.
641 <https://doi.org/10.1080/00288233.1965.10420021>
- 642 Sewell, R. J. (1988a). Late Miocene volcanic stratigraphy of central Banks Peninsula, Canterbury, New Zealand.
643 *New Zealand Journal of Geology and Geophysics*, 31(1), 41-64.
644 <https://doi.org/10.1080/00288306.1988.10417809>
- 645 Sewell, R. J. (1988b). *The volcanic geology and geochemistry of central Banks Peninsula and relationships to*
646 *Lyttelton and Akaroa volcanoes*. (PhD), University of Canterbury, Christchurch.
- 647 Sewell, R. J., Reay, M. B., & Mercury, W. (1993). *Geology of Banks Peninsula. Scale 1:100 000*. Lower Hutt, N.Z.:
648 Institute of Geological and Nuclear Sciences.
- 649 Soil Survey Staff. (1999). *Soil taxonomy* (2nd ed. Vol. 436): United States Department of Agriculture.
- 650 Steefel, C. I., Appelo, C. A. J., Arora, B., Jacques, D., Kalbacher, T., Kolditz, O., et al. (2015). Reactive transport
651 codes for subsurface environmental simulation. *Computational Geosciences*, 19(3), 445-478.
- 652 Stock, B. C., Jackson, A. L., Ward, E. J., Parnell, A. C., Phillips, D. L., & Semmens, B. X. (2018). Analyzing
653 mixing systems using a new generation of Bayesian tracer mixing models. *PeerJ*, 6, e5096
- 654 Stock, B. C., & Semmens, B. X. (2016a). *MixSIAR GUI User Manual*. In. Retrieved from
655 <https://github.com/brianstock/MixSIAR/> doi:10.5281/zenodo.47719
- 656 Stock, B. C., & Semmens, B. X. (2016b). Unifying error structures in commonly used biotracer mixing models.
657 *Ecology*, 97(10), 2562-2569. <https://esajournals.onlinelibrary.wiley.com/doi/abs/10.1002/ecy.1517>
- 658 Tonkin, P. J., & Basher, L. R. (2001). Soil chronosequences in subalpine superhumid Cropp Basin, western
659 Southern Alps, New Zealand. *New Zealand Journal of Geology & Geophysics*, 44, 37-45.
- 660 Trangmar, B. B. (1986). *Soil-landscape relationships Barrys Bay-Wainui District, Banks Peninsula*. Retrieved from
661 <http://doi.org/10.7931/DL1-DOR-CH20>
- 662 Turner, B. L., Hayes, P. E., & Laliberté, E. (2018). A climosequence of chronosequences in southwestern Australia.
663 *European Journal of Soil Science*, 69(1), 69-85. <https://onlinelibrary.wiley.com/doi/abs/10.1111/ejss.12507>
- 664 Turner, S., Mikutta, R., Meyer-Stüve, S., Guggenberger, G., Schaarschmidt, F., Lazar, C. S., et al. (2017). Microbial
665 Community Dynamics in Soil Depth Profiles Over 120,000 Years of Ecosystem Development. *Frontiers in*
666 *Microbiology*, 8(874). Original Research. <https://www.frontiersin.org/article/10.3389/fmicb.2017.00874>
- 667 Viscarra Rossel, R. A., Adamchuk, V. I., Sudduth, K. A., McKenzie, N. J., & Lobsey, C. (2011). Chapter Five -
668 Proximal Soil Sensing: An Effective Approach for Soil Measurements in Space and Time. In D. L. Sparks
669 (Ed.), *Advances in Agronomy* (Vol. 113, pp. 243-291): Academic Press.
- 670 Viscarra Rossel, R. A., McBratney, A. B., & Minasny, B. (2010). *Proximal Soil Sensing*: Springer Netherlands.
- 671 Vitousek, P., Chadwick, O. A., Matson, P., Allison, S., Derry, L., Kettley, L., et al. (2003). Erosion and the
672 Rejuvenation of Weathering-derived Nutrient Supply in an Old Tropical Landscape. *Ecosystems*, 6(8), 762-
673 772.
- 674 Vitousek, P., Dixon, J. L., & Chadwick, O. A. (2016). Parent material and pedogenic thresholds: observations and a
675 simple model. *Biogeochemistry*, 130(1), 147-157. <https://doi.org/10.1007/s10533-016-0249-x>
- 676 Wardle, D. A., Walker, L. R., & Bardgett, R. D. (2004). Ecosystem Properties and Forest Decline in Contrasting
677 Long-Term Chronosequences. *Science*, 305(5683), 509-513.
678 <http://www.sciencemag.org/cgi/content/abstract/305/5683/509>
- 679 Webb, T. H., Campbell, A. S., & Fox, F. B. (1986). Effect of rainfall on pedogenesis in a climosequence of soils
680 near Lake Pukaki, New Zealand. *New Zealand Journal of Geology and Geophysics*, 29(3), 323-334. <https://doi.org/10.1080/00288306.1986.10422155>
- 681 White, A. F., Blum, A. E., Schulz, M. S., Vivit, D. V., Stonestrom, D. A., Larsen, M., et al. (1998). Chemical
682 Weathering in a Tropical Watershed, Luquillo Mountains, Puerto Rico: I. Long-Term Versus Short-Term
683 Weathering Fluxes. *Geochimica et Cosmochimica Acta*, 62(2), 209-226.
684 <http://www.sciencedirect.com/science/article/pii/S0016703797003359>
- 685 Wiesmeier, M., Urbanski, L., Hobbey, E., Lang, B., von Lütow, M., Marin-Spiotta, E., et al. (2019). Soil organic
686 carbon storage as a key function of soils - A review of drivers and indicators at various scales. *Geoderma*,
687 333, 149-162. <https://www.sciencedirect.com/science/article/pii/S0016706117319845>
688

- 689 Yoo, K., Amundson, R., Heimsath, A. M., Dietrich, W. E., & Brimhall, G. H. (2007). Integration of geochemical
690 mass balance with sediment transport to calculate rates of soil chemical weathering and transport on
691 hillslopes. *Journal of Geophysical Research: Earth Surface*, 112(F2), n/a-n/a.
692 <http://dx.doi.org/10.1029/2005JF000402>
- 693 Zhang, Y., Ji, W., Saurette, D. D., Easher, T. H., Li, H., Shi, Z., et al. (2020). Three-dimensional digital soil
694 mapping of multiple soil properties at a field-scale using regression kriging. *Geoderma*, 366, 114253.
695 <https://www.sciencedirect.com/science/article/pii/S0016706119302125>
696